

**Fracture-induced softening in ice dynamics**

T. Albrecht and  
A. Levermann

# Fracture-induced softening for large-scale ice dynamics

T. Albrecht<sup>1,2</sup> and A. Levermann<sup>1,2</sup>

<sup>1</sup>Earth System Analysis, Potsdam Institute for Climate Impact Research, Potsdam, Germany

<sup>2</sup>Institute of Physics and Astronomy, University of Potsdam, Potsdam, Germany

Received: 20 August 2013 – Accepted: 20 August 2013 – Published: 9 September 2013

Correspondence to: A. Levermann (anders.levermann@pik-potsdam.de)

Published by Copernicus Publications on behalf of the European Geosciences Union.

Title Page

Abstract

Introduction

Conclusions

References

Tables

Figures



Back

Close

Full Screen / Esc

Printer-friendly Version

Interactive Discussion

## Abstract

Floating ice shelves can exert a retentive and hence stabilizing force onto the inland ice sheet of Antarctica. However, this effect has been observed to diminish by fracture-coupled dynamic processes within the protective ice shelves leading to accelerated ice flow and hence to a sea-level contribution. In order to better understand the role of fractures in ice dynamics we apply a large-scale continuum representation of fractures and related fracture growth into the prognostic Parallel Ice Sheet Model (PISM). To this end we introduce a higher-order accuracy advection scheme for the transport of the two-dimensional fracture density across the regular computational grid. Dynamic coupling of fractures and ice flow is attained by a reduction of effective ice viscosity proportional to the inferred fracture density. This formulation implies the possibility of a non-linear threshold behavior due to self-amplified fracturing in shear regions triggered by small variations in damage threshold. As a result of prognostic flow simulations, flow patterns with realistically large across-flow velocity gradients in fracture-weakened regions as seen in observations are reproduced. This model framework is expandable to grounded ice streams and accounts for climate-induced effects on fracturing and hence on the ice-flow dynamics. It further allows for an enhanced fracture-based calving parameterization.

## 1 Introduction

The contemporarily observed sea-level change (Cazenave and Llovel, 2010; Church et al., 2011; Gregory et al., 2012) as well as the expected long-term sea-level commitment (Levermann et al., 2013) underpin the role of the contributions of the large polar ice sheets of Greenland and Antarctica (Van den Broeke et al., 2011; Rignot et al., 2011b; Shepherd et al., 2012; Hanna et al., 2013). Reliable and accurate process-based models are required to understand the involved complex processes and to provide confident projections of future sea-level rise (Bamber and Aspinall, 2013). Certain

TCD

7, 4501–4544, 2013

## Fracture-induced softening in ice dynamics

T. Albrecht and  
A. Levermann

Title Page

Abstract

Introduction

Conclusions

References

Tables

Figures

⏪

⏩

◀

▶

Back

Close

Full Screen / Esc

Printer-friendly Version

Interactive Discussion

## Fracture-induced softening in ice dynamics

T. Albrecht and  
A. Levermann

Title Page

Abstract

Introduction

Conclusions

References

Tables

Figures

⏪

⏩

◀

▶

Back

Close

Full Screen / Esc

Printer-friendly Version

Interactive Discussion

aspects of ice flow need a better representation in these models to account for the potential destabilization of key regions, such as the West Antarctic Ice Sheet (Bamber et al., 2009; Joughin and Alley, 2011). The retentive force of floating ice shelves that retains the oceanward ice flow (Dupont and Alley, 2005; Winkelmann et al., 2012; Gudmundsson, 2013) is of high relevance in this assessment. Most models neglect fracture-coupled processes, which can repeal this buttressing effect of ice shelves.

Fracture processes play a fundamental role in the dynamics of ice streams and ice shelves, interacting with external drivers such as ocean melt or atmospheric warming (Pritchard et al., 2012; Rignot et al., 2013; MacAyeal and Sergienko, 2013). Fractures are mostly found as elongated structures of fragments or sequences of troughs and open crevasses, visible at the ice surface. These fracture bands are aligned along the ice flow with origin in the wake of topographic features such as ice rises, ice rumples or along ice stream inlets and usually expand the whole distance towards the calving front. On that journey along the stream, prevailing stresses can change and activate crevasses and rift formation. Such deep-reaching ruptures were observed to propagate horizontally up to 100 km long across flow units (Hulbe et al., 2010).

Fractures and ice flow interact in various ways. Considering one effective direction, certain dynamic regimes promote the formation of fractures. More precisely, they form in regions of strong shear or tensile flow for certain temperature and ice conditions. External forces such as seasonal meltwater drainage can enhance the vertical propagation of existing surface fractures (Weertman, 1973; Van der Veen, 1998a), but snow drift, refreezing or recrystallization can cover and heal them. Similar effects underneath the ice shelf influence the formation and propagation of basal crevasses, which can reach far upward, producing a trough at the surface by viscous adjustment (Van der Veen, 1998b; McGrath et al., 2012b; Luckman et al., 2012; Vaughan et al., 2012). Considering the other effective direction, the abundance of fractures potentially affect the flow regime since horizontal (membrane) stresses cannot be effectively transferred across highly fractured regions due to the loss of mechanical integrity and the reduction of its load-bearing capacity (Borstad et al., 2012, 2013). Inverse modeling provides a

snapshot quantification of the dynamic activity of mechanically weakened areas associated with fractures. Between those partly detached flow units, strong velocity gradients and consequently intense shear is observed, which cannot be reproduced in standard ice-flow models (discussed in Sandhäger et al., 2005; Humbert et al., 2009).

Hence, this interaction of flow and fracture dynamics characterizes a self-amplifying feedback mechanism that is susceptible to changes in external conditions (Scambos et al., 2000, 2003; MacAyeal et al., 2003). Melting and hydro-fracturing causes enhanced structural weakening of the mechanical integrity in fractured regions (Scambos et al., 2009; Glasser and Scambos, 2008; Vieli et al., 2007; Khazendar et al., 2007; Van der Veen, 2007; McGrath et al., 2012a). This reduces the lateral support of the confinement and consequently the buttressing, leading to a speedup of interior ice-shelf flow units, draining more efficiently the upstream glaciers (Rignot et al., 2004; Rott et al., 2011). Stronger shear and thinning in turn supports fracturing, which ultimately can destabilize the entire ice shelf, as observed in several cases along the Antarctic Peninsula (Cook and Vaughan, 2010).

Fracturing of ice represents a key process in the description of the complex ice-flow pattern and plays an important role in ice-shelf calving (Benn et al., 2007) and abrupt disintegration. Particle-flow models may provide a novel and promising representation of fracture formation and related iceberg calving (Bassis and Jacobs, 2013). In this study we present a simplified framework of continuum damage evolution based on ideas by Pralong and Funk (2005) adapted to the finite-difference Parallel Ice Sheet Model (Bueler and Brown, 2009; Winkelmann et al., 2011, based on PISM v.05; see documentation: [www.pism-docs.org](http://www.pism-docs.org)). In the first part we briefly resume the assumptions and methods of identifying regions of fracture initiation and corresponding damage accumulation, which has been described in detail in Albrecht and Levermann (2012). A simple coupling relation of fracture density and viscous-ice deformation is then introduced and justified. Inherent non-linear effects such as multi-stability are exemplarily investigated in a simplified model setup. Applying the proposed fracture-coupling in simulations of several Antarctic ice shelves and comparing the results to observa-

## Fracture-induced softening in ice dynamics

T. Albrecht and  
A. Levermann

[Title Page](#)[Abstract](#)[Introduction](#)[Conclusions](#)[References](#)[Tables](#)[Figures](#)[⏪](#)[⏩](#)[◀](#)[▶](#)[Back](#)[Close](#)[Full Screen / Esc](#)[Printer-friendly Version](#)[Interactive Discussion](#)

tions provides a tool for calibrating employed parameters and thresholds and identifying qualitative differences in the flow field, introduced by the fracture-flow coupling. A concluding discussion summarizes the findings and reveals limitations of the approach and also future applications, such as a fracture-induced calving parameterization.

## 2 The fracture density concept

The basic idea of the continuous, dynamically evolving fracture-density field, applied to ice shelves, has been introduced by Albrecht and Levermann (2012). The scalar value of the isotropic damage variable,  $0 \leq \phi \leq 1$ , called “fracture density”, has been interpreted as a measure for the density of macroscopic but subgrid-scale fracture features per ice-shelf area. As a field variable,  $\phi$  can be transported with the ice flow  $\mathbf{v}$  as

$$\frac{\partial \phi}{\partial t} + \mathbf{v} \cdot \nabla \phi = f_s + f_h. \quad (1)$$

In this simple advection equation  $f_s$  and  $f_h$  indicate the source and sink terms.

In areas, where a certain fracture-initiation threshold  $\sigma_{cr}$  is exceeded,  $\phi$  is assumed to grow with a rate that is proportional to the local maximum spreading rate,  $\dot{e}_+$ . This functional relationship accounts for the probability for the initiation of new fractures within a grid cell area and hence for fracture accumulation. Since brittle fractures, e.g., surface and bottom crevasses, are likely produced in previously cracked regimes, we here consider the aggregated effect, not distinguishing between individual fracture representations. The presence of densely-spaced fractures however restricts the probability for additional fracture formation by reducing the overall stress field in their proximity, which is expressed simply by a reducing factor,  $1 - \phi$ , in the damage evolution function

$$f_s = \begin{cases} \gamma \cdot \dot{e}_+ \cdot (1 - \phi), & \sigma_t \geq \sigma_{cr} \\ 0, & \sigma_t < \sigma_{cr} \end{cases}. \quad (2)$$

## Fracture-induced softening in ice dynamics

T. Albrecht and  
A. Levermann

Title Page

Abstract

Introduction

Conclusions

References

Tables

Figures

⏪

⏩

◀

▶

Back

Close

Full Screen / Esc

Printer-friendly Version

Interactive Discussion





distinct dynamic characteristics. From a macroscopic point of view, this dynamic decoupling corresponds to a softening effect of the ice that can be expressed in the model as a modified flow-enhancement factor  $E_A$  (Humbert, 2006; Humbert et al., 2009). Assuming the strain-equivalence between physical and effective spaces (Pralong and Funk, 2005; Duddu and Waisman, 2012a; Borstad et al., 2013), the stress-balance equation remains unchanged with a modified effective viscosity defined as

$$\eta_\phi = E_A^{-\frac{1}{n}} \cdot \left[ \frac{1}{2} \cdot \dot{\epsilon}_e^{\frac{1-n}{n}} \int B(T) dz \right]. \quad (5)$$

Here,  $B(T)$  denotes ice hardness (or rigidity), which depends on the vertical temperature distribution,  $T = T(z)$ . The effective strain rate,  $\dot{\epsilon}_e$ , is the second invariant of the strain-rate tensor (equivalent to the effective stress in Eq. (3)), with  $n = 3$ , Glen's flow law parameter.

We assume a simple functional relationship for the fracture-density induced softening, written as

$$E_A = E_{SSA} \cdot [1 - (1 - \varepsilon) \cdot \phi]^{-n} \xrightarrow{\varepsilon=0} E_{SSA} \cdot [1 - \phi]^{-n}. \quad (6)$$

For its implementation in the numerical model we introduce the parameter  $\varepsilon$  as a lower limit for the softening, avoiding a degeneration of the equations. In the simulations presented here epsilon is  $\varepsilon = 0.001$ . The SSA-enhancement factor,  $E_{SSA}$ , is commonly used in ice modeling and comprises anisotropy and other softening effects of the intact ice (Ma et al., 2010; Winkelmann et al., 2011). However,  $E_{SSA}$  is taken to be constant in space and time.

The influence of the two unitless parameters on the emerging non-linear coupling is shown in Fig. 1. For a fracture density of  $\phi = 0.5$  and, hence half the undamaged viscosity, ice is softened by a factor  $E_A = 5$  up to  $E_A = 8$ . This is realistic for commonly used rate factors  $E_{SSA}$  (left-hand panel). Due to the strong non-linearity, this factor is almost an order of magnitude larger ( $35 \leq E_A \leq 60$ ) for a fracture density of  $\phi = 0.75$  and a quarter of the undistorted ice viscosity. This illustrates the pathway into discontinuous

## Fracture-induced softening in ice dynamics

T. Albrecht and  
A. Levermann

Title Page

Abstract

Introduction

Conclusions

References

Tables

Figures

⏪

⏩

◀

▶

Back

Close

Full Screen / Esc

Printer-friendly Version

Interactive Discussion



behavior approaching vanishing viscosity, which seems ambiguous in the framework of continuum mechanics. In this regime of fracture densities close to 1, the comparably small residual value  $\varepsilon$  limits ice softness to guarantee convergence of the stress balance calculation. The proposed functional relationship is a crude estimate based on plausibility arguments and needs to be quantitatively characterized.

The proposed model framework implies a potentially self-amplifying feedback mechanism: If fractures form in a certain region, the ice will be softened according to Eq. (6), which allows for a concentration of shear. This applies also in regions downstream of the formation area where the fractures are transported to. Stronger shear increases the effective stress and if the initiation threshold is hit, additional fractures can form leading to an increasing fracture density there. Healing and numerical diffusion counteract the accumulation of damage, which otherwise would tend to approach asymptotically the upper bounding value 1.

## 4 Methods

### 4.1 Evaluating fracture initiation criteria

Failure of ice occurs at stresses beyond certain thresholds and is hence often expressed in terms of material strength. There is a variety of phenomenological standard failure criteria for the identification of regions where fracturing potentially occurs. We use the von-Mises criterion based on the maximum effective stress exceeding a critical value (Eq. 3), which is equivalent to the exceedance of a maximal distortion energy (von Mises, 1913; Vaughan, 1993). This criterion is very similar to the maximum shear stress criterion (a.k.a. Tresca or Guest criterion in literature)

$$\sigma_{ms} = \max(|\sigma_+|, |\sigma_-|, |\sigma_+ - \sigma_-|). \quad (7)$$

In a computational setup of the Larsen C Ice Shelf with a resolution of 1.75 km, this maximum shear stress is about 15% larger than the effective stress used in the von-

## Fracture-induced softening in ice dynamics

T. Albrecht and  
A. Levermann

Title Page

Abstract

Introduction

Conclusions

References

Tables

Figures

⏪

⏩

◀

▶

Back

Close

Full Screen / Esc

Printer-friendly Version

Interactive Discussion



Mises criterion (Fig. 2 b, e). If the corresponding threshold is reduced by 15% with respect to the von-Mises strength ( $\sigma_t \geq 70$  kPa and  $\sigma_{ms} \geq 80$  kPa coincide with 95%) fracture formation is initiated in the same regions and very similar steady-state patterns of fracture density evolve.

A more sophisticated fracture-initiation criterion, derived from Linear Elastic Fracture Mechanics (LEFM), takes into account both shear and tensile modes of cracking in a biaxial stress field. Following this approach, a single crevasse forms when the critical fracture toughness  $K_{Ic}$  is exceeded by the combined stress intensities, defined as

$$K_{Ic} \leq \sqrt{\pi c} \left[ \sigma_n \cos^3 \left( \frac{\theta}{2} \right) + \tau_s \cos \left( \frac{\theta}{2} \right) \sin(\theta) \right], \quad (8)$$

$$\text{with } \theta = -2 \arctan \left( \frac{\sqrt{\sigma_n^2 + 8 \tau_s^2} - \sigma_n}{4 \tau_s} \right). \quad (9)$$

The parameter  $c$  denotes the half-length of preexisting edge cracks,  $\sigma_n$  is the stress across to the crack opening and  $\tau_s$  the shear stress along the crack planes (see Erdogan and Sih (1963); Shyam Sunder and Wu (1990); Rist et al. (1999); Hulbe et al. (2010) for details). The fracture toughness for a given geometry of preexisting flaws is density-dependent. For the low-density firm at the surface, a fracture toughness of  $K_{Ic} \approx 50 \text{ kPa} \sqrt{\text{m}}$  was obtained in laboratory experiments with ice core specimen from the Ronne Ice Shelf (Rist et al., 1999, 2002). Larger values of  $K_{Ic} \approx 150 \text{ kPa} \sqrt{\text{m}}$  or more are expected for the meteoric or marine ice at the ice shelf bottom. For fracture fields of narrow-spaced crevasses, the fracture toughness can even be twice or triple as high as for intact ice (Van der Veen, 1998a). It appears that the initial crack half-length  $c$  is a weakly confined parameter. We assigned a value of  $c = 0.2$  m, such that the root mean square error in comparison to the von-Mises criterion becomes minimal within the computational setup of the Larsen C region (Fig. 2 f). Jansen et al. (2010) indicate a unique pattern of potential crevasse opening for a given ratio of fracture toughness and half-length, which compares very well with Fig. 2 c, (compare violet contour lines

Fracture-induced softening in ice dynamics

T. Albrecht and A. Levermann

Title Page

Abstract

Introduction

Conclusions

References

Tables

Figures

⏪

⏩

◀

▶

Back

Close

Full Screen / Esc

Printer-friendly Version

Interactive Discussion



## Fracture-induced softening in ice dynamics

T. Albrecht and  
A. Levermann

Title Page

Abstract

Introduction

Conclusions

References

Tables

Figures

⏪

⏩

◀

▶

Back

Close

Full Screen / Esc

Printer-friendly Version

Interactive Discussion

of  $50 \text{ kPa} \sqrt{\text{m}}$ ). Since the relevant brittle fracture-formation areas coincide mostly with those identified with the ductile von-Mises criterion (for  $K_{Ic} = 70 \text{ kPa} \sqrt{\text{m}}$  and  $\sigma_t \geq 70 \text{ kPa}$  fracture-formation area have a 75% match), the fracture density pattern does not show major differences at the resolutions applied here. Hence, in the following study we use the von-Mises criterion only.

A similar approach based on LEFM was proposed by Van der Veen (1998a,b) for the investigation of vertical crack propagation of both surface and bottom crevasses but only for tensile crack modes. An accurate estimate of the maximal fracture depth requires accurate data of the vertical profiles of ice density and other physical parameters (Rist et al., 2002; Plate et al., 2012). This approach of vertical fracture extension will not be further discussed in this study and might be part of future studies.

### 4.2 Feature-preserving two-dimensional numerical advection scheme

Standard first-order upstream differencing schemes are a commonly applied pragmatic choice to approximate hyperbolic-type partial differential equations as the advection equation in Eq. (1) (e.g., Press et al., 2009). However, these schemes are known to be numerically dissipative. Especially for plane flow that is oblique with respect to the underlying grid (“zigzag” course from cell to cell), it tends to smear out well-defined structures of high fracture density on their way downstream, which can be associated with an angle-dependent healing for unphysical reasons. Therefore we implemented an upstream transport scheme of higher-order accuracy such that the gradient, corresponding to the smaller vector velocity component, is shifted upstream, considering

eight different cases depending on the flow angle,

$$\phi_{N+1} = \phi_N - \Delta t \cdot \begin{cases} u(\phi_{i,j} - \phi_{i-1,j})/\Delta x + v(\phi_{i-1,j} - \phi_{i-1,j-1})/\Delta y, & 0 \leq v\Delta x/\Delta y \leq u \\ u(\phi_{i,j-1} - \phi_{i-1,j-1})/\Delta x + v(\phi_{i,j} - \phi_{i,j-1})/\Delta y, & 0 \leq u\Delta y/\Delta x \leq v \\ -u(\phi_{i,j-1} - \phi_{i+1,j-1})/\Delta x + v(\phi_{i,j} - \phi_{i,j-1})/\Delta y, & 0 \geq u\Delta y/\Delta x \geq -v \\ -u(\phi_{i,j} - \phi_{i+1,j})/\Delta x + v(\phi_{i+1,j} - \phi_{i+1,j-1})/\Delta y, & 0 \leq v\Delta x/\Delta y \leq -u \\ -u(\phi_{i,j} - \phi_{i+1,j})/\Delta x - v(\phi_{i+1,j} - \phi_{i+1,j+1})/\Delta y, & 0 \geq v\Delta x/\Delta y \geq u \\ -u(\phi_{i,j+1} - \phi_{i+1,j+1})/\Delta x - v(\phi_{i,j} - \phi_{i,j+1})/\Delta y, & 0 \geq u\Delta y/\Delta x \geq v \\ u(\phi_{i,j+1} - \phi_{i-1,j+1})/\Delta x - v(\phi_{i,j} - \phi_{i,j+1})/\Delta y, & 0 \leq u\Delta y/\Delta x \geq -v \\ u(\phi_{i,j} - \phi_{i-1,j})/\Delta x - v(\phi_{i-1,j} - \phi_{i-1,j+1})/\Delta y, & 0 \geq v\Delta x/\Delta y \geq -u, \end{cases} \quad (10)$$

where  $N$  indicates the time step while  $i$  and  $j$  are the coordinates on the regular rectangular grid (see Fig. 3). This modification improves the representation of advection in two dimensions and exhibits much less numerical diffusion for transport that is oblique with respect to the grid axes. Figure 4 shows three transects perpendicular and along the symmetry flowline in a simplified ice-shelf setup of 100 km width and length. Fracture density as a tracer is initialized with unity value within a small domain of  $8 \times 8$  km. Theoretically a narrow band of constant fracture density is expected downstream. In fact, if the flow direction coincides with one grid axis, numerical diffusion can be neglected for both schemes (Fig. 4 a). When turning the main flow direction by  $45^\circ$  the higher order scheme reveals a very high accuracy as in the unturned case. In contrast, for the first order scheme, maximum values are reduced to about 40% of its initial value over a distance of 90 km (dashed profile in Fig. 4 b). For the flow that is turned by intermediate angles, such as  $22.5^\circ$ , both schemes show an unintended numerical diffusion, but significantly less for the higher-order accuracy upstream scheme (solid profile in Fig. 4 c). Higher resolution increases the accuracy significantly for both schemes (Fig. 5), which has to be considered in the experiments.

### 4.3 Fracture formation along grounded ice streams

Fractures are often observed to be initiated in the rocky shear margins of the inlets upstream from the grounding line, where ice flow accelerates due to decreased basal friction. The boundary condition for the fracture-density evolution,  $\phi_0$ , is applied along the grounding line that confines the ice shelf domain. In this way,  $\phi_0$ , accounts for pre-existing fractures draining through the inlets. We assume that fracture processes in grounded but “shelfy” regions occur under similar conditions as within the ice shelf domain. In this way we can calculate contributions to the fracture density field from observed velocities in the grounded regions as prescribed boundary condition along the grounding line, yielding a more realistic  $\phi_0$  than in a previous study.

### 4.4 Interpreting fracture density from satellite visible imagery

In order to compare the modeled fracture density with observations, we hand-digitized visible surface features that seem to represent fracture phenomena of any kind. We identified these features in MOA satellite spectroradiometer images of the largest Antarctic ice shelves as snapshot of the years 2003 to 2004 (Scambos et al., 2007, MODIS Mosaic of Antarctica). Recent observation have shown that observed surface troughs in ice shelves often correspond to widely spaced basal crevasses, which support surface fracturing by viscous-adjustment induced bending effects (McGrath et al., 2012b; Luckman et al., 2012; Vaughan et al., 2012). However, the smaller surface crevasses as well as the highly fragmented shear zones are hard to identify from satellite data for resolutions of 150 m, especially when snow-covered. Here we do not distinguish between the different representations (Glasser and Scambos, 2008; Glasser et al., 2009).

Following Albrecht and Levermann (2012), we calculated a two-dimensional representation of the observed fracture features,  $\phi_{\text{obs}}$ , for each grid cell of a given resolution, assuming a rectangular “zone of influence” of 1 km width. This assumption is moti-

TCD

7, 4501–4544, 2013

## Fracture-induced softening in ice dynamics

T. Albrecht and  
A. Levermann

Title Page

Abstract

Introduction

Conclusions

References

Tables

Figures

◀

▶

◀

▶

Back

Close

Full Screen / Esc

Printer-friendly Version

Interactive Discussion

vated by the fact that, for crevasse opening perpendicular to the the main tensile stress axis, the applied far-field stress has to circumvent the discontinuity. This reduces the effective stress to both sides of the crack, acting as a stress shadow cast.

Additionally, the inferred observed fracture density was smoothed with a running mean along the flowline, which is derived from the modeled/observed velocity field. This along-flowline spatial smoothing of the monitored snapshot mimics a time average and reveals more clearly the continuous band structure of observed fractures, e.g., in suture zones and along shear margins (see Fig. 6). Apparently, this mapping procedure cannot give a precise and complete picture of the dynamically relevant observed fracture regions, but it gives an impression of the rough pattern of fracture abundance and accumulation for a qualitative validation.

## 4.5 Computational setup and settings

The simulations of the Antarctic ice shelves that we performed are based on high-resolution datasets. Ice thickness, bed-topography data and the grounding-line position are described in the Bedmap2 product on a 1 km grid in polar stereographic projection (Fretwell et al., 2013). In order to avoid grounding in shallow ice-shelf areas, the sub-shelf seabed elevation is arbitrarily set to 2000 m depth. Climatic mass balance and ice-surface temperature are available from ALBMAP v1 on a 5 km grid (Le Brocq et al., 2010). FESOM data (melting and refreezing rates beneath the ice shelf), averaged over the historical period 1960 to 1999, were kindly provided on an unstructured grid with resolutions of up to 4 km by Timmermann et al. (2012); Timmermann and Hellmer (2013). Surface-velocity data covering the whole Antarctic continent has been assembled by Rignot et al. (2011a) from multiple satellite interferometric radar data of the years 2007 to 2009. The data are used for validation and as Dirichlet boundary conditions along the grounding line (and in some subregions along the boundaries of the computational domain if the flow is directed inwards).

## Fracture-induced softening in ice dynamics

T. Albrecht and  
A. Levermann

Title Page

Abstract

Introduction

Conclusions

References

Tables

Figures

⏪

⏩

◀

▶

Back

Close

Full Screen / Esc

Printer-friendly Version

Interactive Discussion



**Fracture-induced  
softening in ice  
dynamics**T. Albrecht and  
A. Levermann

Title Page

Abstract

Introduction

Conclusions

References

Tables

Figures

◀

▶

◀

▶

Back

Close

Full Screen / Esc

Printer-friendly Version

Interactive Discussion

Since the datasets are a product of a period after the breakup of Larsen A and B Ice Shelves, the input data has been modified for this region according to a period prior to it (Jezek et al., 2003, Modified Antarctic Mapping Mission (MAMM)). Initial ice thickness in the embayment was inferred from surface elevation data on a 2 km grid with applied firn-correction (Lythe et al., 2001). Provided MAMM surface velocities of the time period 1997 to 2000 for validation exhibit gaps that has been filled using an SOR method for the Laplace equation. For the inlets Dirichlet boundary conditions are based on the latest observations by Rignot et al. (2011a).

For the computational setup of the Pine Island and Thwaites region the boundary is defined along the inner-continental ice divide separating the drainage basin. Within this basin the stress balance is solved additionally in Shallow Ice Approximation (SIA) superposing the SSA for a prescribed basal friction field, which is a combination of PISM-internal parameterizations (Winkelmann et al., 2011) and inversely inferred data, provided courtesy of Ian Joughin.

Iceberg calving is not considered in the simulations. The ice flow is simply cut off at the initial ice-shelf front. Friction along side margins and ice rises is not explicitly set as in previous studies since it inherently results from ice thickness and velocity along the boundary. Fracture initiation is considered also in the grounded region as determined by the prescribed velocities based on observations and is transported across the grounding line into the ice-shelf domain. Density within the ice is prescribed with a constant value of  $910 \text{ kg m}^{-3}$ .

A simplified computational setup is used with an ice shelf confined in a rectangular bay of 100 km width and 2000 m depth. Constant ice inflow is defined at the upper grounding line with 600 m thickness and  $300 \text{ m yr}^{-1}$  speed while the side margins are ice-free walls. Surface temperature is constantly  $-30^\circ \text{C}$  and surface-mass balance  $0.1 \text{ m yr}^{-1}$  on the ice shelf. The minimum resolution is 1 km in this simplified setup, which can be simply rescaled to coarser multiples of that resolution.

## 5 Results

### 5.1 Self-amplified fracturing

Non-linear systems may exhibit bistable phenomena based on a positive, i.e. self-amplifying, feedback loop as proposed previously in the text (Sect. 3). On large climatic scales, systems that exhibit such behavior are sometimes called “tipping elements” (Levermann et al., 2011). Here this characteristic behavior is investigated in a simplified experiment where within a confined ice shelf region (a few grid cells) fracture density of  $\phi = 0.7$  is prescribed, which imitates a constantly active fracture source. The damaged ice is carried with the flow downstream and decays slightly by diffusive healing as long as the effective stress stays below the fracture-initiation threshold,  $\sigma_{cr}$ . If this spot is situated in a shearing flow field, the damage-induced softening intensifies the shear and hence the effective stress. In the experiment we gradually decrease  $\sigma_{cr}$ , which corresponds to additional forcing supporting fracture formation, such as meltwater infiltration. If the effective stress hits a specific threshold (here  $\sigma_{cr} < 80$  kPa) additional fractures form and accumulate downstream of the initial point (see the jump in Fig. 7). This in turn increases the effective stress in this confined area, leading to the plotted steady state profiles. If environmental conditions reverse, such that the fracture threshold  $\sigma_{cr}$  increases, we observe a jump back to the former state of a weakly decaying fracture band for  $\sigma_{cr} > 82$  kPa, thus revealing a classic hysteresis behavior. This is a robust feature and is also found in more realistic setups representing relevant Antarctic Ice Shelves.

### 5.2 Application to Antarctic ice shelves and subregions

In the following the various aspects of fracture-softening are investigated in exemplary ice shelf sub-regions of the largest Ross and Ronne-Filchner Ice Shelves (see colored rectangles in Fig. 6). The smaller northern-most Larsen Ice Shelves along the Antarctic Peninsula and the Pine Island Glacier will be discussed as separate cases. Simulations

TCD

7, 4501–4544, 2013

## Fracture-induced softening in ice dynamics

T. Albrecht and  
A. Levermann

Title Page

Abstract

Introduction

Conclusions

References

Tables

Figures

⏪

⏩

◀

▶

Back

Close

Full Screen / Esc

Printer-friendly Version

Interactive Discussion

are performed on a 1 km regular grid. Parameters are roughly estimated such that the qualitative changes become apparent for each individual setup.

### 5.2.1 Byrd Inlet in Ross Ice Shelf

The Byrd inlet is an important inflow for the Ross Ice Shelf, draining through a narrow trough of the Transantarctic mountains (Fig. 8 a). From there the ice flows as a homogeneous unit at about  $600 \text{ m yr}^{-1}$  eastwards through slow moving ice that is confined within the embayment of Ross Island. The cross section right after the entrance of the inlet shows steep velocity gradients especially on the northern side. A constant flow enhancement  $E_{\text{SSA}} = 0.4$  yields reasonable results for simulations of the whole Ross Ice Shelf domain. The corresponding profile perpendicular to the main flow direction, however, shows a smooth transition between the broad inflow unit and the much slower surrounding ice (light blue in Fig. 8 c), but it does not allow for the intense observed shear flow. In contrast, fracture-softening reveals highly fractured bands on both sides of the inlet (Fig. 8 b), confining the fast flow unit, with strong gradients at its flanks (violet profile in Fig. 8 c). However, the resulting profile appears to be shifted transversally by about 15 km, which might be caused by underestimated inflow through the southern boundary of the computational domain, which forces the incoming stream northwards. The orange contour lines in Fig. 8 b indicate that fractures form already in the grounded upstream inlet channel, where the von-Mises effective stress is larger than 110 kPa. This fracture band partly detaches the flow from the topographical promontory further downstream (Pr), which otherwise would act as fracture-formation area. Healing is comparably small but fracture density vanishes within about 100 km distance as suggested by observations in this area. The basic flow enhancement for intact ice in the remaining computational domain is very much reduced ( $E_{\text{SSA}} = 0.05$ ) in order to match the observed plateau in flow speed within the dynamically separated flow unit.

## Fracture-induced softening in ice dynamics

T. Albrecht and  
A. Levermann

Title Page

Abstract

Introduction

Conclusions

References

Tables

Figures

◀

▶

◀

▶

Back

Close

Full Screen / Esc

Printer-friendly Version

Interactive Discussion



## 5.2.2 Evans Inlet in Ronne Ice Shelf

The ice stream of the Evans Glacier enters the second largest Ronne Ice Shelf in the west and turns north. This motion yields an inclined cross profile with a speed of up to  $700 \text{ m yr}^{-1}$  at the souther margin jumping to almost  $100 \text{ m yr}^{-1}$  in some minor side inlets (green profile in Fig. 9 d). Simulations with ordinary stress balance require a small basic flow enhancement  $E_{SSA} = 0.1$  (light blue in Fig. 9 c,d), in order to reproduce observed surface velocities in this region. However, neither the inclination of the main flow nor the strong gradient at the southern flank are well represented. Fracture-softening instead exhibits these features and produces a thin fracture band along the rocky margin. From there the fracture zone continues with the main flow and separates the stagnant regions at the sides (right hand side in Fig. 9 d). A relatively high fracture toughness of 140 kPa and a comparably strong healing in the main trunk of the inlet limits the extent of the fracture band and restricts the inflow in the observed range. Observations confirm the presence of elongated fragmental structures close to the margin from where crevasses propagate towards the center line of the inlet.

## 5.2.3 Filchner Ice Shelf

Filchner Ice Shelf is the fastest of the smaller Antarctic ice shelves with speeds up to  $1400 \text{ m yr}^{-1}$  close to the front (Fig. 10 a). It shears along Berkner Ice Rise (BIR) at its western margin and drains into the Weddel Sea in the north. The cross section is located south of the rifted areas at the north-eastern margin (cf. Fig. 6 b and Fig. 10 c). The maximum speed is shifted from the center line towards the Berkner side with a small buckle at about 70 km distance. This feature likely indicates the presence of a suture zone between the flow unit fed by the Recovery and the flow coming from the Support Force Glacier farther west. The characteristic flow pattern in relation to observed surface crevasses was already diagnostically studied by Saheicha et al. (2006), presuming a crevasse band with origin at Recovery Glacier inlet (see overlain structures in Fig. 10 b). Simulations with constant enhancement factor  $E_{SSA} = 0.4$  produce

### Fracture-induced softening in ice dynamics

T. Albrecht and  
A. Levermann

Title Page

Abstract

Introduction

Conclusions

References

Tables

Figures

⏪

⏩

◀

▶

Back

Close

Full Screen / Esc

Printer-friendly Version

Interactive Discussion



5 a symmetric and smooth velocity distribution within the Filchner trough (light blue in Fig. 10c). A much better representation of elongated structures such as the suture zone representation within the main trunk causing a small kink in the velocity profile is provided by application of the fracture-softening scheme with a relatively high fracture toughness of 130 kPa. For chosen parameters, best agreement with observations is attained with a reduced enhancement for unfractured ice of  $E_{SSA} = 0.2$ , reproducing much of the inclination and the steep gradient at the western margin. The straight inclined part of the observed profile might be an effect of the rift system downstream, which is not accounted for in the model.

10 The characteristic fracture band pattern is also obtained for lower resolution of 2 km or even 5 km (Fig. 11), however much more damped for wider meshes (cf. Fig. 5). Hence the softening effect is weaker and the typical shape of the across velocity profile is less pronounced.

### 5.2.4 Larsen B Region prior to its break-up

15 The Larsen B Ice Shelf is situated at the north-eastern flank of the Antarctic Peninsula facing the Weddel Sea (Fig. 12). The climatic conditions in this region are considerably different from those in the more continental ice shelves farther south. Surface melting during summer can produce melt ponds (Glasser and Scambos, 2008), which initiate a series of processes that can result in such large-scale events as the disintegration of major parts of Larsen B in 2002 within a few weeks (Rack and Rott, 2004). Satellite observations indicated a heavily crevassed ice-shelf surface prior to the collapse (Fig. 6c) and model studies confirmed the dynamically active role of those fractured regions (Sandhäger, 2003; Sandhäger et al., 2005; Vieli et al., 2006, 2007; Khazendar et al., 2007; Borstad et al., 2012). Since ordinary model configurations with constant flow enhancement fail to accurately reproduce the characteristic pre-collapse flow pattern with steep velocity gradients across weak shear zones along the side margins of the Larsen B regime (cf. green profile in Fig. 12), our fracture density approach provides a physically motivated tool to reduce this discrepancy. The velocity of the interior

## Fracture-induced softening in ice dynamics

T. Albrecht and  
A. Levermann

Title Page

Abstract

Introduction

Conclusions

References

Tables

Figures

⏪

⏩

◀

▶

Back

Close

Full Screen / Esc

Printer-friendly Version

Interactive Discussion



## Fracture-induced softening in ice dynamics

T. Albrecht and  
A. Levermann

Title Page

Abstract

Introduction

Conclusions

References

Tables

Figures

⏪

⏩

◀

▶

Back

Close

Full Screen / Esc

Printer-friendly Version

Interactive Discussion

of the ice shelf appears plateau-shaped. This can be explained by the partial mechanical decoupling from the confining side margins such that a large enhancement factor of  $E_{SSA} = 10$  is needed to reach observed maximum velocity values of up to  $560 \text{ m yr}^{-1}$  along the central front (cf. dashed light blue in Fig. 12 e). Especially along inlets close to the grounding line the computed velocities are far too small (Fig. 12 f).

A damage-dependent and hence spatially varying flow enhancement reproduces the observations much better (thick violet in Fig. 12 e,f), since the inferred fracture density identifies the dynamically relevant weak zones and allows for intense localized softening and hence strong flow gradients. This applies even for enhancement factor  $E_{SSA} = 1.0$  as base level for unfractured ice, which is glaciologically more realistic than values larger than 1. A comparably high value for the fracture rate  $\gamma = 1.0$  and a low value of the fracture-initiation threshold  $\sigma_t = 60 \text{ kPa}$  is needed in order to yield high damage accumulation close to unit value and hence strong softening in the active regions. Especially within the narrow tributary inlets, densely spaced fractures and hence intense softening occurs, which coincides with detailed observation in these areas (Glasser and Scambos, 2008, Fig. 2). Surface meltwater draining into existing crevasses and enhancing fracture formation support this parameter choice. On the other hand, for accumulation rates of more than  $1 \text{ m yr}^{-1}$  and possibly refreezing within surface and bottom crevasses, strong healing  $\gamma_h = 2.0$  may be plausible. In this parameter setting the healing threshold  $\dot{\epsilon}_h = 6 \times 10^{-10} \text{ s}^{-1}$  becomes a sensitive parameter separating fracture-free regions from those of self-amplified fracture weakening.

### 5.2.5 Pine Island and Thwaites drainage basin

The Amundson Sea sector with the Pine Island Glacier is one of the key regions in the discussion on sea-level rise. Large portions of the West Antarctic Ice Sheet are drained through this confined fast outlet. Pine Island ice shelf is subjected to enhanced ocean melt and has accelerated by about 50% in the last decade, propagating upstream (Joughin et al., 2003, 2010; Scott et al., 2009; Warner and Roberts, 2013). Velocity computations with a constant enhancement factor of  $E_{SSA} = 0.8$  provide a rea-

## Fracture-induced softening in ice dynamics

T. Albrecht and  
A. Levermann

Title Page

Abstract

Introduction

Conclusions

References

Tables

Figures

⏪

⏩

◀

▶

Back

Close

Full Screen / Esc

Printer-friendly Version

Interactive Discussion

sonable agreement with observations of surface velocities by Rignot et al. (2011a). However, the fast-flowing portions in the lower Pine Island ice stream and in the ice shelf are underestimated (peaking up to  $4000 \text{ m yr}^{-1}$ , see Fig. 13). We applied the fracture-softening method in a simulation of the Pine Island and Thwaites region in order to demonstrate its effects in a dynamically coupled ice sheet - ice stream - ice shelf system. The procedure identifies fracture zones at the margins of the fast-flowing ice-stream regions leading to an acceleration there. In fact, fractures are visible at the surface and may play an interactive role in the complex dynamics of Pine Island Glacier. In this specific setting, fracture initiation thresholds of  $\sigma_t \leq 90 \text{ kPa}$  can initiate a run-away feedback, where fracture-induced acceleration and thinning promote grounding line retreat (see sketch in Fig. 13 c). This ungrounding leads to even more acceleration, expansion and shearing, which intensifies in turn fracturing. This phenomenon is worth a separate study but will not be discussed further here.

## 6 Discussion

Fractured regions in a shear zone can support only limited stress and lose this ability when crossing a specific threshold. Fracture-induced softening has the potential to introduce non-linear characteristics into the ice-flow dynamics such as dynamic regime shifts (bifurcation) and hysteresis (irreversibility). This has been investigated for steady-state configurations with respect to successively varied parameters (Fig. 7). A self-amplifying process is then activated and additional fractures intensify the shear, which in turn promotes additional fracturing. Hence, small changes in environmental conditions potentially have strong impacts in such systems. A short surface-melting period can trigger a change in fracture threshold and may activate such abrupt shifts between dynamic regimes. This mechanism is robust and may occur for different settings at different thresholds. Critical effective stresses of  $80 \text{ kPa}$  as in the demonstrated simplified case are found at the lower end of the observation-derived critical-value range with values reaching up to  $320 \text{ kPa}$ . This large range indicates a high variability of fracture

histories, temperature regimes, ice properties but also uncertainty in the conversion of measurable strain-rates to stresses (Vaughan, 1993). Hence, stress thresholds are not constant material parameters and may differ depending on various conditions.

However, independent of this qualitative possibility of non-linear threshold behavior, we find that the influence of fractures on the creep of ice is relevant in a number of situations. This study does not aim at a conclusive investigation of the influence of fracture on the flow field, but is meant to introduce the concept and provide results on the qualitative changes in the flow field when fracture density is accounted for. The critical strengths for the realistic computational setups of Antarctic ice shelves were determined such that characteristic observed flow patterns are adequately represented, which provides a rough way of parameter calibration. The so estimated critical values for the large Antarctic ice shelves are located in the lower half of this literature range, i.e., 110 kPa–140 kPa (Fig. 8–10). In contrast a comparably low threshold of 60 kPa was chosen in the smaller Larsen B Ice Shelf situated at the Antarctic Peninsula (Fig. 12). This is counter-intuitive since warmer ice is supposed to support higher stresses before failure. However, using higher thresholds in the simulation cannot produce the degree of damage within the evolving fracture bands, which is necessary to capture the observed strong shearing for the given setting of enhancement factor and healing parameters,  $E_{SSA}$ ,  $\gamma_h$  and  $\dot{\epsilon}_h$  respectively. External conditions like melt water draining into surface crevasses or basal melting intensified within basal crevasses openings provide reasonable explanations for a considerably lower threshold in this region. However, this study is not meant as a parameter-tuning exercise and the inferred parameters should be considered with caution. Generally, for increasing basic enhancement factor  $E_{SSA}$ , stresses are intensified throughout the ice shelf domain and thresholds are more likely hit at stress maxima. Related ice-shelf thinning is not further discussed here. The signal of fracture softening in ice thickness is much less pronounced than in flow speeds.

In our study we used the von-Mises criterion, which identifies preferably fracture initiation in shear regions. We have shown that more sophisticated mixed-mode criteria based on LEFM do not change the results significantly, at least for large-scale simu-

## Fracture-induced softening in ice dynamics

T. Albrecht and  
A. Levermann

[Title Page](#)[Abstract](#)[Introduction](#)[Conclusions](#)[References](#)[Tables](#)[Figures](#)[⏪](#)[⏩](#)[◀](#)[▶](#)[Back](#)[Close](#)[Full Screen / Esc](#)[Printer-friendly Version](#)[Interactive Discussion](#)

## Fracture-induced softening in ice dynamics

T. Albrecht and  
A. Levermann

Title Page

Abstract

Introduction

Conclusions

References

Tables

Figures

⏪

⏩

◀

▶

Back

Close

Full Screen / Esc

Printer-friendly Version

Interactive Discussion

lations of ice shelves. Since tensile crevassing occurs predominantly in pre-fractured ice, we do not distinguish between the particular failure behavior and assume a smooth transition of ductile to brittle fracturing. In the present formulation we account for horizontal interactions simply parameterized by a factor  $(1 - \phi)$  in Eq. (2), bounding the evolving fracture density. However, this integrated view neglects the vertical extent and possibly non-linear interactions of basal and surface crevasses (McGrath et al., 2012b,a; Luckman et al., 2012; Vaughan et al., 2012). In fact, the vertical dimension of fracturing is relevant in understanding fracture interaction and calving and needs to be specified in an expanded formulation for the fracture density. To give an example, tensile crevasse formation at the ice-shelf bottom triggered by vertical bending at the grounding line (Logan et al., 2013) cannot be captured by shallow approximation models. Contribution of such processes may be considered as boundary conditions,  $\phi_0$ , in future studies. Considering the involved vertical bending stresses, tidal flexure seem to play a secondary role.

The presented method locates the areas that are most susceptible to fracture formation. With origin in these spots, elongated damage bands often reach far downstream towards the front. Viscosity is reduced along these confined fractured zones assuming a linear relationship, comprising all relevant softening processes (including micro-scale dynamic recrystallization or damage-induced anisotropy). This procedure mimics a partial mechanical decoupling of the so-separated regions and reproduces a couple of observed flow characteristics: Fast-flowing units of the ice shelf pass by stagnant ice shelf regions in minor side bays (Fig. 9 and 12) or get sutured together with neighboring flow units of different speed. This can be identified by jumps or kinks in ice-speed cross-section (Figs. 8 and 10). Ice-stream inlets shearing along the rocky fjord walls accelerate when the main flow gets partly detached from the sticky margins (Figs. 9 and 13). Similar effects are observed within small ice shelves shearing along islands or ice rises. Along these fractured zones of weakness transversal stresses cannot be transferred effectively leading to increased speed and less buttressing. Observations of fracture features at the surface provide an incomplete picture. That is, dynamically



fracture-density approach provides a spatial and temporal link between small-scale fracture initiation and post-formation processes occurring on the large scale and eventually located elsewhere. Rift propagation and calving would be examples of such phenomena. Hence, the structural integrity and stability of key regions, buttressing the ice flow, can be evaluated in a more realistic manner and potential contributions to global sea level can be assessed with more confidence.

*Acknowledgements.* We thank Ed Bueler, Constantine Khroulev and David Maxwell (University of Alaska, USA) for a great collaboration and technical assistance with the Parallel Ice Sheet Model (PISM), development of which is supported by NASA grants NNX09AJ38C, NNX13AM16G, and NNX13AK27G. We are grateful for stimulating discussions with Guillaume Jouvét. We also thank Matthias Mengel for preprocessing various datasets. Ralph Timmermann kindly provided FESOM sub-shelf melting data and Neil Glasser detailed observational surface feature maps of the Larsen Ice Shelves. T. A. was funded by the German National Merit Foundation (Studienstiftung des deutschen Volkes).

## References

- Albrecht, T. and Levermann, A.: Fracture field for large-scale ice dynamics, *J. Glaciol.*, 58, 2012. 4504, 4505, 4506, 4512
- Bamber, J. L. and Aspinall, W. P.: An expert judgement assessment of future sea level rise from the ice sheets, *Nature Climate Change*, 3, 424–427, doi:10.1038/nclimate1778, 2013. 4502
- Bamber, J. L., Riva, R. E. M., Vermeersen, B. L. A., and LeBrocq, A. M.: Reassessment of the Potential Sea-Level Rise from a Collapse of the West Antarctic Ice Sheet, *Science*, 324, 901–903, doi:10.1126/science.1169335, <http://www.sciencemag.org/cgi/doi/10.1126/science.1169335>, 2009. 4503
- Bassis, J. N. and Jacobs, S.: Diverse calving patterns linked to glacier geometry, *Nat. Geosci.*, advance online publication, doi:10.1038/ngeo1887, 2013. 4504
- Bassis, J. N., Fricker, H. A., Coleman, R., and Minster, J. B.: An investigation into the forces that drive ice-shelf rift propagation on the Amery Ice Shelf, East Antarctica, *J. Glaciol.*, 54, 17–27, 2008. 4523

## Fracture-induced softening in ice dynamics

T. Albrecht and  
A. Levermann

Title Page

Abstract

Introduction

Conclusions

References

Tables

Figures

⏪

⏩

◀

▶

Back

Close

Full Screen / Esc

Printer-friendly Version

Interactive Discussion



## Fracture-induced softening in ice dynamics

T. Albrecht and  
A. Levermann

Title Page

Abstract

Introduction

Conclusions

References

Tables

Figures

◀

▶

◀

▶

Back

Close

Full Screen / Esc

Printer-friendly Version

Interactive Discussion



- Benn, D. I., Warren, C. R., and Mottram, R. H.: Calving processes and the dynamics of calving glaciers, *Earth-Sci. Rev.*, 82, 143–179, 2007. 4504
- Borstad, C. P., Khazendar, A., Larour, E., Morlighem, M., Rignot, E., Schodlok, M. P., and Seroussi, H.: A damage mechanics assessment of the Larsen B ice shelf prior to collapse: Toward a physically-based calving law, *Geophys. Res. Lett.*, 39, L18502, <http://www.agu.org/pubs/crossref/2012/2012GL053317.shtml>, 2012. 4503, 4506, 4518, 4523
- Borstad, C. P., Rignot, E., Mouginot, J., and Schodlok, M. P.: Creep deformation and buttressing capacity of damaged ice shelves: theory and application to Larsen C ice shelf, *The Cryosphere Discussions*, 7, 3567–3610, doi:10.5194/tcd-7-3567-2013, 2013. 4503, 4507, 4523
- Bueler, E. and Brown, J.: Shallow shelf approximation as a “sliding law” in a thermomechanically coupled ice sheet model, *J. Geophys. Res.*, 114, F03008, 2009. 4504
- Cazenave, A. and Llovel, W.: Contemporary sea level rise, *Annu. Rev. Mar. Sci.*, 2, 145–173, <http://www.annualreviews.org/doi/abs/10.1146/annurev-marine-120308-081105>, 2010. 4502
- Church, J., White, N., Konikow, L., Domingues, C., Cogley, J., Rignot, E., Gregory, J., van den Broeke, M., Monaghan, A., and Velicogna, I.: Revisiting the Earth’s sea-level and energy budgets from 1961 to 2008, *Geophys. Res. Lett.*, 38, L18601, 2011. 4502
- Cook, A. J. and Vaughan, D. G.: Overview of areal changes of the ice shelves on the Antarctic Peninsula over the past 50 years, *The Cryosphere*, 4, 77–98, doi:10.5194/tc-4-77-2010, 2010. 4504
- Duddu, R. and Waisman, H.: A temperature dependent creep damage model for polycrystalline ice, *Mechanic. Material.*, 46, 23–41, doi:10.1016/j.mechmat.2011.11.007, 2012a. 4506, 4507
- Duddu, R. and Waisman, H.: A nonlocal continuum damage mechanics approach to simulation of creep fracture in ice sheets, *Comput. Mechanic.*, 51, 961–974, doi:10.1007/s00466-012-0778-7, 2012b. 4506
- Dupont, T. K. and Alley, R. B.: Assessment of the importance of ice-shelf buttressing to ice-sheet flow, *Geophys. Res. Lett.*, 32, L04503, 2005. 4503
- Erdogan, F. and Sih, G.: On the crack extension in plates under plane loading and transverse shear, *J. Basic Eng.*, 85, 519–527, 1963. 4509
- Fretwell, P., Pritchard, H. D., Vaughan, D. G., Bamber, J. L., Barrand, N. E., Bell, R., Bianchi, C., Bingham, R. G., Blankenship, D. D., Casassa, G., Catania, G., Callens, D., Conway, H., Cook, A. J., Corr, H. F. J., Damaske, D., Damm, V., Ferraccioli, F., Forsberg, R., Fujita, S.,

**Fracture-induced  
softening in ice  
dynamics**T. Albrecht and  
A. Levermann

Title Page

Abstract

Introduction

Conclusions

References

Tables

Figures

◀

▶

◀

▶

Back

Close

Full Screen / Esc

Printer-friendly Version

Interactive Discussion

Gim, Y., Gogineni, P., Griggs, J. A., Hindmarsh, R. C. A., Holmlund, P., Holt, J. W., Jacobel, R. W., Jenkins, A., Jokat, W., Jordan, T., King, E. C., Kohler, J., Krabill, W., Riger-Kusk, M., Langley, K. A., Leitchenkov, G., Leuschen, C., Luyendyk, B. P., Matsuoka, K., Mouginot, J., Nitsche, F. O., Nogi, Y., Nost, O. A., Popov, S. V., Rignot, E., Rippin, D. M., Rivera, A.,  
5 Roberts, J., Ross, N., Siegert, M. J., Smith, A. M., Steinhage, D., Studinger, M., Sun, B., Tinto, B. K., Welch, B. C., Wilson, D., Young, D. A., Xiangbin, C., and Zirizzotti, A.: Bedmap2: improved ice bed, surface and thickness datasets for Antarctica, *The Cryosphere*, 7, 375–393, doi:10.5194/tc-7-375-2013, 2013. 4513

10 Glasser, N. F. and Scambos, T. A.: A structural glaciological analysis of the 2002 Larsen B ice-shelf collapse, *J. Glaciol.*, 54, 3–16, 2008. 4504, 4512, 4518, 4519

Glasser, N. F., Kulesa, B., Luckman, A., Jansen, D., King, E. C., Sammonds, P. R., Scambos, T. A., and Jezek, K. C.: Surface structure and stability of the Larsen C ice shelf, Antarctic Peninsula, *J. Glaciol.*, 55, 400–410, 2009. 4512

15 Gregory, J. M., White, N. J., Church, J. A., Bierkens, M. F. P., Box, J. E., van den Broeke, M. R., Cogley, J. G., Fettweis, X., Hanna, E., Huybrechts, P., Konikow, L. F., Leclercq, P. W., Marzeion, B., Oerlemans, J., Tamisiea, M. E., Wada, Y., Wake, L. M., and van de Wal, R. S.: Twentieth-century global-mean sea-level rise: is the whole greater than the sum of the parts?, *J. Climate*, p. 121203145300007, doi:10.1175/JCLI-D-12-00319.1, 2012. 4502

20 Gudmundsson, G. H.: Ice-shelf buttressing and the stability of marine ice sheets, *The Cryosphere*, 7, 647–655, doi:10.5194/tc-7-647-2013, 2013. 4503

Habermann, M., Maxwell, D., and Truffer, M.: Reconstruction of basal properties in ice sheets using iterative inverse methods, *J. Glaciol.*, 58, 795–807, doi:10.3189/2012JoG11J168, 2012. 4523

25 Hanna, E., Navarro, F. J., Pattyn, F., Domingues, C. M., Fettweis, X., Ivins, E. R., Nicholls, R. J., Ritz, C., Smith, B., Tulaczyk, S., Whitehouse, P. L., and Zwally, H. J.: Ice-sheet mass balance and climate change, *Nature*, 498, 51–59, doi:10.1038/nature12238, 2013. 4502

Hulbe, C. L., LeDoux, C., and Cruikshank, K.: Propagation of long fractures in the Ronne Ice Shelf, Antarctica, investigated using a numerical model of fracture propagation, *J. Glaciol.*, 56, 459–472, 2010. 4503, 4509, 4523

30 Humbert, A.: Numerical simulations of the ice flow dynamics of Fimbulisen, in: FRISP Report, Vol. 17, 2006. 4507

## Fracture-induced softening in ice dynamics

T. Albrecht and  
A. Levermann

Title Page

Abstract

Introduction

Conclusions

References

Tables

Figures

⏪

⏩

◀

▶

Back

Close

Full Screen / Esc

Printer-friendly Version

Interactive Discussion



- Humbert, A., Kleiner, T., Mohrholz, C. O., Oelke, C., Greve, R., and Lange, M. A.: A comparative modeling study of the Brunt Ice Shelf/Stancomb-Wills Ice Tongue system, East Antarctica, *J. Glaciol.*, 55, 53–65, 2009. 4504, 4507
- Jansen, D., Kulesa, B., Sammonds, P. R., Luckman, A., King, E., and Glasser, N. F.: Present stability of the Larsen C ice shelf, Antarctic Peninsula, *J. Glaciol.*, 56, 593–600, 2010. 4509
- Jezek, K. C., Farness, K., Carande, R., Wu, X., and Labelle-Hamer, N.: RADARSAT 1 synthetic aperture radar observations of Antarctica: Modified Antarctic Mapping Mission, 2000, *Radio Science*, 38, 8067, <http://bprc.osu.edu/rsl/radarsat/data/mamm/>, 2003. 4514
- Joughin, I. and Alley, R. B.: Stability of the West Antarctic ice sheet in a warming world, *Nat. Geosci.*, 4, 506–513, doi:10.1038/ngeo1194, 2011. 4503
- Joughin, I., Rignot, E., Rosanova, C. E., Lucchitta, B. K., and Bohlander, J.: Timing of recent accelerations of Pine island glacier, Antarctica, *Geophys. Res. Lett.*, 30, 1706, 2003. 4519
- Joughin, I., Smith, B. E., and Holland, D. M.: Sensitivity of 21st century sea level to ocean-induced thinning of Pine Island Glacier, Antarctica, *Geophys. Res. Lett.*, 37, L20502, 2010. 4519
- Khazendar, A., Rignot, E., and Larour, E.: Larsen B Ice Shelf rheology preceding its disintegration inferred by a control method, *Geophys. Res. Lett.*, 34, L19503, 2007. 4504, 4518, 4523
- Le Brocq, A. M., Payne, A. J., Griggs, J., Nitsche, F., Shapiro, N., Van den Broeke, M., and Vaughan, D.: An improved Antarctic dataset for high resolution numerical ice sheet models (ALBMAP v1), <http://doi.pangaea.de/10.1594/PANGAEA.734145>, 2010. 4513
- Levermann, A., Bamber, J. L., Drijfhout, S., Ganopolski, A., Haeberli, W., Harris, N. R. P., Huss, M., Krüger, K., Lenton, T. M., Lindsay, R. W., Notz, D., Wadhams, P., and Weber, S.: Potential climatic transitions with profound impact on Europe, *Climat. Change*, doi:10.1007/s10584-011-0126-5, 2011. 4515
- Levermann, A., Albrecht, T., Winkelmann, R., Martin, M. A., Haseloff, M., and Joughin, I.: Kinematic first-order calving law implies potential for abrupt ice-shelf retreat, *The Cryosphere*, 6, 273–286, doi:10.5194/tc-6-273-2012, 2012. 4523
- Levermann, A., Clark, P. U., Marzeion, B., Milne, G. A., Pollard, D., Radic, V., and Robinson, A.: The multimillennial sea-level commitment of global warming, *P. Natl. Acad. Sci.*, doi:10.1073/pnas.1219414110, 2013. 4502
- Logan, L., Catania, G., Lavier, L., and Choi, E.: A novel method for predicting fracture in floating ice, *J. Glaciol.*, 59, 750–758, doi:10.3189/2013JoG12J210, 2013. 4522

## Fracture-induced softening in ice dynamics

T. Albrecht and  
A. Levermann

Title Page

Abstract

Introduction

Conclusions

References

Tables

Figures

⏪

⏩

◀

▶

Back

Close

Full Screen / Esc

Printer-friendly Version

Interactive Discussion



- Luckman, A., Jansen, D., Kulesa, B., King, E. C., Sammonds, P., and Benn, D. I.: Basal crevasses in Larsen C Ice Shelf and implications for their global abundance, *The Cryosphere*, 6, 113–123, doi:10.5194/tc-6-113-2012, 2012. 4503, 4512, 4522
- Lythe, M. B., Vaughan, D. G., and the BEDMAP Consortium, : BEDMAP: A new ice thickness and subglacial topographic model of Antarctica, *J. Geophys. Res. B.*, 106, 11335–11351, 2001. 4514
- Ma, Y., Gagliardini, O., Ritz, C., Gillet-Chaulet, F., Durand, G., and Montagnat, M.: Enhancement factors for grounded ice and ice shelves inferred from an anisotropic ice-flow model, *J. Glaciol.*, 56, 805, 2010. 4507
- MacAyeal, D. and Sergienko, O. V.: The flexural dynamics of melting ice shelves, *Ann. Glaciol.*, 54, 1, <http://www.igsoc.org/annals/54/63/t63A256.pdf>, 2013. 4503
- MacAyeal, D. R., Scambos, T. A., Hulbe, C. L., and Fahnestock, M. A.: Catastrophic ice-shelf break-up by an ice-shelf-fragment-capsize mechanism, *J. Glaciol.*, 49, 22–36, 2003. 4504
- McGrath, D., Steffen, K., Rajaram, H., Scambos, T., Abdalati, W., and Rignot, E.: Basal crevasses on the Larsen C Ice Shelf, Antarctica: Implications for meltwater ponding and hydrofracture, *Geophys. Res. Lett.*, 39, L16504, doi:10.1029/2012GL052413, 2012a. 4504, 4522
- McGrath, D., Steffen, K., Scambos, T., Rajaram, H., Casassa, G., and Lagos, J.: Basal crevasses and associated surface crevassing on the Larsen C ice shelf, Antarctica, and their role in ice-shelf instability, *Ann. Glaciol.*, 58, 60, 2012b. 4503, 4512, 4522
- Plate, C., Müller, R., Humbert, A., and Gross, D.: Evaluation of the criticality of cracks in ice shelves using finite element simulations, *The Cryosphere*, 6, 973–984, doi:10.5194/tc-6-973-2012, 2012. 4510
- Pralong, A. and Funk, M.: Dynamic damage model of crevasse opening and application to glacier calving, *J. Geophys. Res.*, 110, B01309, 2005. 4504, 4506, 4507
- Press, W. H., Teukolsky, S. A., Vetterling, W. T., and Flannery, B. P.: Numerical recipes in C++: the art of scientific computing, Vol. 994, Cambridge University Press Cambridge, 2009. 4510
- Pritchard, H. D., Ligtenberg, S. R. M., Fricker, H. A., Vaughan, D. G., van den Broeke, M. R., and Padman, L.: Antarctic ice-sheet loss driven by basal melting of ice shelves, *Nature*, 484, 502–505, doi:10.1038/nature10968, 2012. 4503
- Rack, W. and Rott, H.: Pattern of retreat and disintegration of the Larsen B ice shelf, Antarctic Peninsula, *Ann. Glaciol.*, 39, 505–510, 2004. 4518

## Fracture-induced softening in ice dynamics

T. Albrecht and  
A. Levermann

Title Page

Abstract

Introduction

Conclusions

References

Tables

Figures

⏪

⏩

◀

▶

Back

Close

Full Screen / Esc

Printer-friendly Version

Interactive Discussion

- Rignot, E., Casassa, G., Gogineni, P., Krabill, W., Rivera, A., and Thomas, R.: Accelerated ice discharge from the Antarctic Peninsula following the collapse of Larsen B ice shelf, *Geophys. Res. Lett.*, 31, 18, 2004. 4504
- 5 Rignot, E., Mouginot, J., and Scheuchl, B.: Ice Flow of the Antarctic Ice Sheet, *Science*, 333, 1427–1430, doi:10.1126/science.1208336, <http://nsidc.org/data/nsidc-0484.html>, 2011a. 4513, 4514, 4520
- Rignot, E., Velicogna, I., van den Broeke, M. R., Monaghan, A., and Lenaerts, J.: Acceleration of the contribution of the Greenland and Antarctic ice sheets to sea level rise, *Geophys. Res. Lett.*, 38, L05503, 2011b. 4502
- 10 Rignot, E., Jacobs, S., Mouginot, J., and Scheuchl, B.: Ice Shelf Melting Around Antarctica, *Science*, doi:10.1126/science.1235798, 2013. 4503
- Rist, M. A., Sammonds, P. R., Murrell, S. A. F., Meredith, P. G., Doake, C. S. M., Oerter, H., and Matsuki, K.: Experimental and theoretical fracture mechanics applied to Antarctic ice fracture and surface crevassing, *J. Geophys. Res.*, 104, 2973–2987, 1999. 4509
- 15 Rist, M. A., Sammonds, P. R., Oerter, H., and Doake, C. S. M.: Fracture of Antarctic shelf ice, *J. Geophys. Res.*, 107, 2002. 4509, 4510
- Rott, H., Müller, F., Nagler, T., and Floricioiu, D.: The imbalance of glaciers after disintegration of Larsen-B ice shelf, *Antarctic Peninsula, The Cryosphere*, 5, 125–134, doi:10.5194/tc-5-125-2011, 2011. 4504
- 20 Saheicha, K., Sandhäger, H., and Lange, M. A.: Modelling the Flow Regime of Filchner-Schelfeis, *FRISP Rep*, 14, 58–62, 2006. 4517
- Sandhäger, H.: Numerical study on the influence of fractures and zones of weakness on the flow regime of Larsen Ice Shelf, in: *FRISP Report*, Vol. 14, 2003. 4518
- Sandhäger, H., Rack, W., and Jansen, D.: Model investigations of Larsen B Ice Shelf dynamics prior to the breakup, in: *FRISP Report*, Vol. 16, 5–7, 2005. 4504, 4518
- 25 Scambos, T., Hulbe, C., and Fahnestock, M.: Climate-induced ice shelf disintegration in the Antarctic Peninsula, *Antarc. Res. Ser.*, 79, 79–92, [http://web.pdx.edu/~chulbe/science/reprints/ScambosHulbeFahne\\_ARS03.pdf](http://web.pdx.edu/~chulbe/science/reprints/ScambosHulbeFahne_ARS03.pdf), 2003. 4504
- Scambos, T., Haran, T., Fahnestock, M., Painter, T., and Bohlander, J.: MODIS-based Mosaic of Antarctica (MOA) data sets: Continent-wide surface morphology and snow grain size, *Remote Sens. Environ.*, 111, 242–257, doi:10.1016/j.rse.2006.12.020, <http://nsidc.org/data/nsidc-0280.html>, 2007. 4512, 4537
- 30

## Fracture-induced softening in ice dynamics

T. Albrecht and  
A. Levermann

Title Page

Abstract

Introduction

Conclusions

References

Tables

Figures

◀

▶

◀

▶

Back

Close

Full Screen / Esc

Printer-friendly Version

Interactive Discussion

- Scambos, T., Fricker, H. A., Liu, C. C., Bohlander, J., Fastook, J., Sargent, A., Massom, R., and Wu, A. M.: Ice shelf disintegration by plate bending and hydro-fracture: Satellite observations and model results of the 2008 Wilkins ice shelf break-ups, *Earth Planet. Sci. Lett.*, 280, 51–60, 2009. 4504
- 5 Scambos, T. A., Hulbe, C., Fahnestock, M., and Bohlander, J.: The link between climate warming and break-up of ice shelves in the Antarctic Peninsula, *J. Glaciol.*, 46, 516–530, 2000. 4504
- Scott, J. B. T., Gudmundsson, G. H., Smith, A. M., Bingham, R. G., Pritchard, H. D., and Vaughan, D. G.: Increased rate of acceleration on Pine Island Glacier strongly coupled to changes in gravitational driving stress, *The Cryosphere*, 3, 125–131, doi:10.5194/tc-3-125-2009, 2009. 4519
- 10 Shepherd, A., Ivins, E. R., A, G., Barletta, V. R., Bentley, M. J., Bettadpur, S., Briggs, K. H., Bromwich, D. H., Forsberg, R., Galin, N., Horwath, M., Jacobs, S., Joughin, I., King, M. A., Lenaerts, J. T. M., Li, J., Ligtenberg, S. R. M., Luckman, A., Luthcke, S. B., McMillan, M., Meister, R., Milne, G., Mouginit, J., Muir, A., Nicolas, J. P., Paden, J., Payne, A. J., Pritchard, H., Rignot, E., Rott, H., Sørensen, L. S., Scambos, T. A., Scheuchl, B., Schrama, E. J. O., Smith, B., Sundal, A. V., Angelen, J. H. v., Berg, W. J. v. d., Broeke, M. R. v. d., Vaughan, D. G., Velicogna, I., Wahr, J., Whitehouse, P. L., Wingham, D. J., Yi, D., Young, D., and Zwally, H. J.: A Reconciled Estimate of Ice-Sheet Mass Balance, *Science*, 338, 1183–1189, doi:10.1126/science.1228102, 2012. 4502
- 15 Shyam Sunder, S. and Wu, M. S.: Crack nucleation due to elastic anisotropy in polycrystalline ice, *Cold Regions Science and Technology*, 18, 29–47, 1990. 4509
- Timmermann, R. and Hellmer, H.: Southern Ocean warming and increased ice shelf basal melting in the twenty-first and twenty-second centuries based on coupled ice-ocean finite-element modelling, *Ocean Dynam.*, Springer Heidelberg, 1–16, doi:10.1007/s10236-013-0642-0, 2013. 4513
- 25 Timmermann, R., Wang, Q., and Hellmer, H.: Ice shelf basal melting in a global finite-element sea ice/ice shelf/ocean model, *Ann. Glaciol.*, 53, http://epic.awi.de/24946/, 2012. 4513
- Van den Broeke, M. R., Bamber, J., Lenaerts, J., and Rignot, E.: Ice Sheets and Sea Level: Thinking Outside the Box, *Surveys in geophysics*, 1–11, 2011. 4502
- 30 Van der Veen, C. J.: Fracture mechanics approach to penetration of surface crevasses on glaciers, *Cold Regions Science and Technology*, 27, 31–47, 1998a. 4503, 4509, 4510

## Fracture-induced softening in ice dynamics

T. Albrecht and  
A. Levermann

Title Page

Abstract

Introduction

Conclusions

References

Tables

Figures

◀

▶

◀

▶

Back

Close

Full Screen / Esc

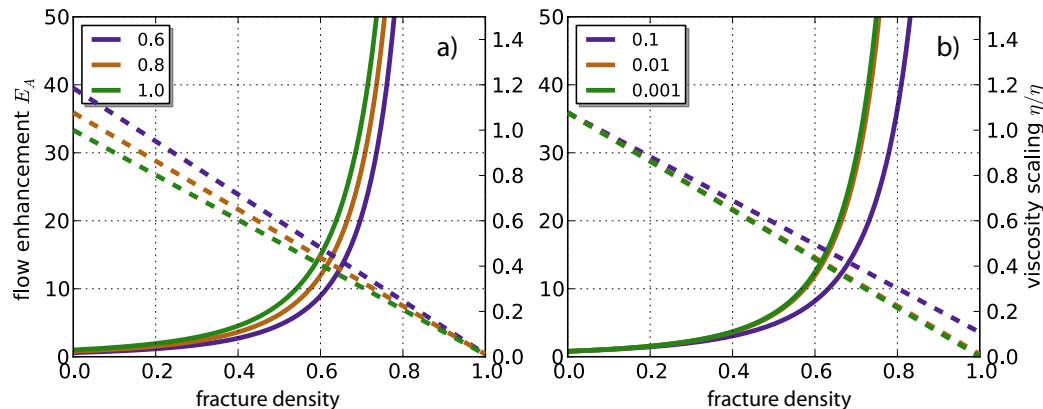
Printer-friendly Version

Interactive Discussion

- Van der Veen, C. J.: Fracture mechanics approach to penetration of bottom crevasses on glaciers, *Cold Regions Science and Technology*, 27, 213–223, 1998b. 4503, 4510
- Van der Veen, C. J.: Fracture propagation as means of rapidly transferring surface meltwater to the base of glaciers, *Geophys. Res. Lett.*, 34, L01501, 2007. 4504
- 5 Vaughan, D. G.: Relating the occurrence of crevasses to surface strain rates, *J. Glaciol.*, 39, 255–266, 1993. 4506, 4508, 4521
- Vaughan, D. G., Corr, H. F. J., Bindschadler, R. A., Dutrieux, P., Gudmundsson, G. H., Jenkins, A., Newman, T., Vornberger, P., and Wingham, D. J.: Subglacial melt channels and fracture in the floating part of Pine Island Glacier, Antarctica, *J. Geophys. Res.*, 117, F03012, doi:10.1029/2012JF002360, 2012. 4503, 4512, 4522
- 10 Vieli, A., Payne, A. J., Du, Z., and Shepherd, A.: Numerical modelling and data assimilation of the Larsen B ice shelf, Antarctic Peninsula, *Philos. T. R. Soc. A.*, 364, 1815, 2006. 4518
- Vieli, A., Payne, A. J., Shepherd, A., and Du, Z.: Causes of pre-collapse changes of the Larsen B ice shelf: Numerical modelling and assimilation of satellite observations, *Earth Planet. Sci. Lett.*, 259, 297–306, 2007. 4504, 4518
- 15 von Mises, R.: *Mechanik der festen Körper im plastisch deformablen Zustand*, Göttingen. *Nachr. Math. Phys.*, 1, 582–592, 1913. 4506, 4508
- Warner, R. C. and Roberts, J. L.: Pine Island Glacier (Antarctica) velocities from Landsat7 images between 2001 and 2011: FFT-based image correlation for images with data gaps, *J. Glaciol.*, 59, 571–582, doi:10.3189/2013JoG12J113, 2013. 4519
- 20 Weertman, J.: Can a water-filled crevasse reach the bottom surface of a glacier, *IASH Publ.*, 95, 139–145, 1973. 4503
- Winkelmann, R., Martin, M. A., Haseloff, M., Albrecht, T., Bueller, E., Khroulev, C., and Levermann, A.: The Potsdam Parallel Ice Sheet Model (PISM-PIK) – Part 1: Model description, *The Cryosphere*, 5, 715–726, doi:10.5194/tc-5-715-2011, 2011. 4504, 4507, 4514
- 25 Winkelmann, R., Levermann, A., Martin, M. A., and Frieler, K.: Increased future ice discharge from Antarctica owing to higher snowfall, *Nature*, 492, 239–242, doi:10.1038/nature11616, 2012. 4503

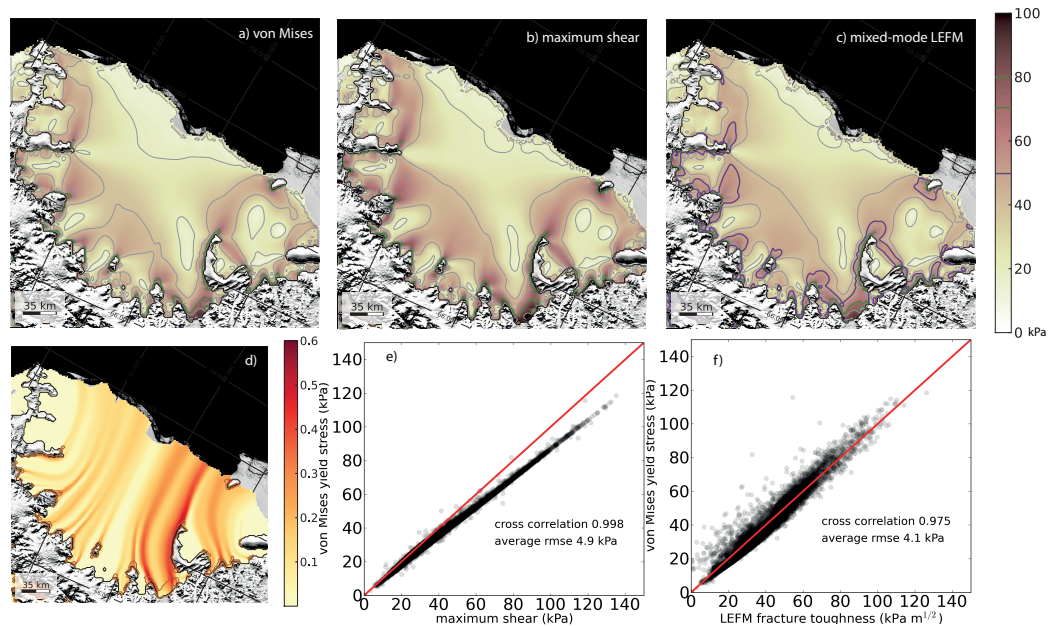
## Fracture-induced softening in ice dynamics

T. Albrecht and  
A. Levermann



**Fig. 1.** Functional relationship of ice softening (left axis) and viscosity (dashed lines associated with right axis) with respect to fracture density as in Eq. (6) is shown for commonly used SSA-enhancement factors  $E_{SSA}$  **(a)** and residual parameter  $\varepsilon$  **(b)**.

[Title Page](#)
[Abstract](#)
[Introduction](#)
[Conclusions](#)
[References](#)
[Tables](#)
[Figures](#)
[◀](#)
[▶](#)
[◀](#)
[▶](#)
[Back](#)
[Close](#)
[Full Screen / Esc](#)
[Printer-friendly Version](#)
[Interactive Discussion](#)

Fracture-induced  
softening in ice  
dynamicsT. Albrecht and  
A. Levermann

**Fig. 2.** Comparison of von-Mises effective stress, maximum-shear stress and LEFM-stress intensity in the Larsen C Ice Shelf region with green contours at 70 kPa, 80 kPa and  $70 \text{ kPa} \sqrt{\text{m}}$  respectively. Resultant steady-state fracture density is shown in the lower left panel, no healing or softening applied. Scatter plots show the point-wise comparison for the given examples in the lower right panels.

Title Page

Abstract

Introduction

Conclusions

References

Tables

Figures

◀

▶

◀

▶

Back

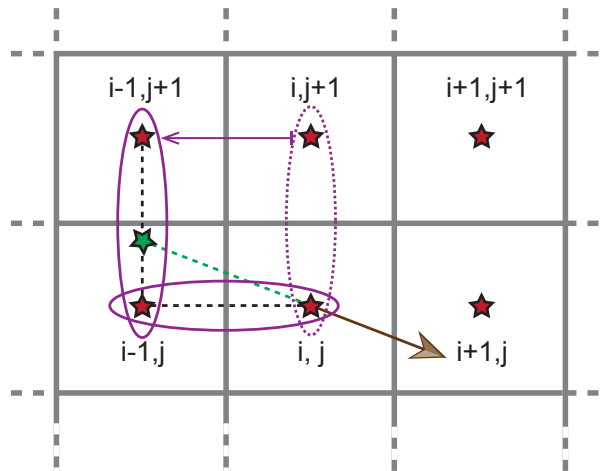
Close

Full Screen / Esc

Printer-friendly Version

Interactive Discussion

## Fracture-induced softening in ice dynamics

T. Albrecht and  
A. Levermann

**Fig. 3.** Two-dimensional view of grid cell  $i, j$  with a brown velocity vector pointing to the lower right cell neighbors ( $0 \geq v_{i,j} \Delta x / \Delta y \geq -u_{i,j}$ ). The first-order upwind scheme takes into account the gradients along the two axes between the direct neighboring cells. In order to gain a higher accuracy the second gradient is shifted upstream (violet arrow). This improved scheme mimics a velocity-weighted gradient along the green-dashed flowline.

Title Page

Abstract

Introduction

Conclusions

References

Tables

Figures

◀

▶

◀

▶

Back

Close

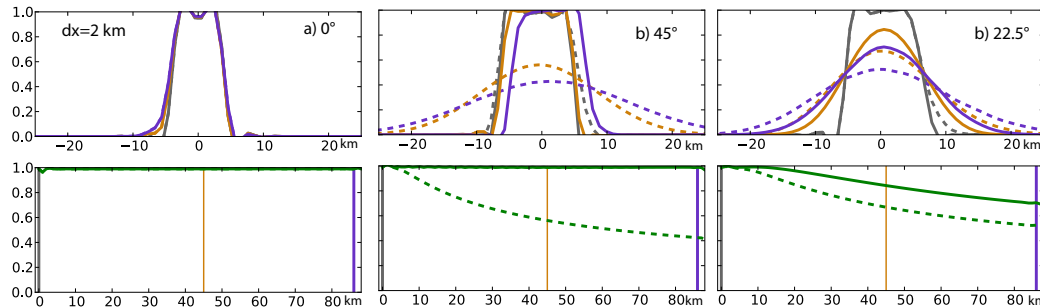
Full Screen / Esc

Printer-friendly Version

Interactive Discussion

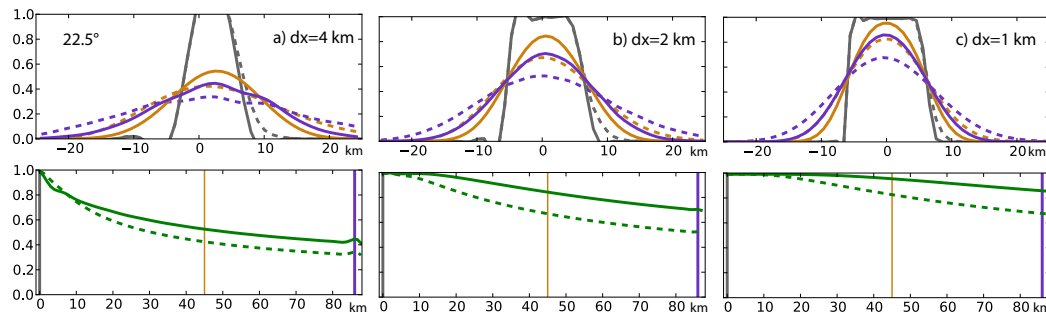
## Fracture-induced softening in ice dynamics

T. Albrecht and  
A. Levermann



**Fig. 4.** Dissipation of fracture density during transport as studied in a simplified ice-shelf setup where the main flow direction is  $0^\circ$ ,  $45^\circ$  and  $22.5^\circ$  oblique with respect to the underlying regular grid of mesh width 2 km. The top-panels show three transecting profiles through the steady-state fracture-density field perpendicular to the main flow direction (bivariate interpolation). Dashed lines represent the first-order upstream scheme used so far, solid lines the higher-order-accuracy scheme. In the bottom panels the corresponding dissipative decay along the flow direction is plotted for both schemes. Vertical lines show location of top-panel transects.

[Title Page](#)
[Abstract](#)
[Introduction](#)
[Conclusions](#)
[References](#)
[Tables](#)
[Figures](#)
[◀](#)
[▶](#)
[◀](#)
[▶](#)
[Back](#)
[Close](#)
[Full Screen / Esc](#)
[Printer-friendly Version](#)
[Interactive Discussion](#)

**Fracture-induced  
softening in ice  
dynamics**T. Albrecht and  
A. Levermann

**Fig. 5.** Transport of fracture density as in Fig. 3 for different mesh sizes 4 km, 2 km and 1 km where the main flow direction is turned by  $22.5^\circ$  with respect to the underlying regular grid.

[Title Page](#)[Abstract](#)[Introduction](#)[Conclusions](#)[References](#)[Tables](#)[Figures](#)[⏪](#)[⏩](#)[◀](#)[▶](#)[Back](#)[Close](#)[Full Screen / Esc](#)[Printer-friendly Version](#)[Interactive Discussion](#)

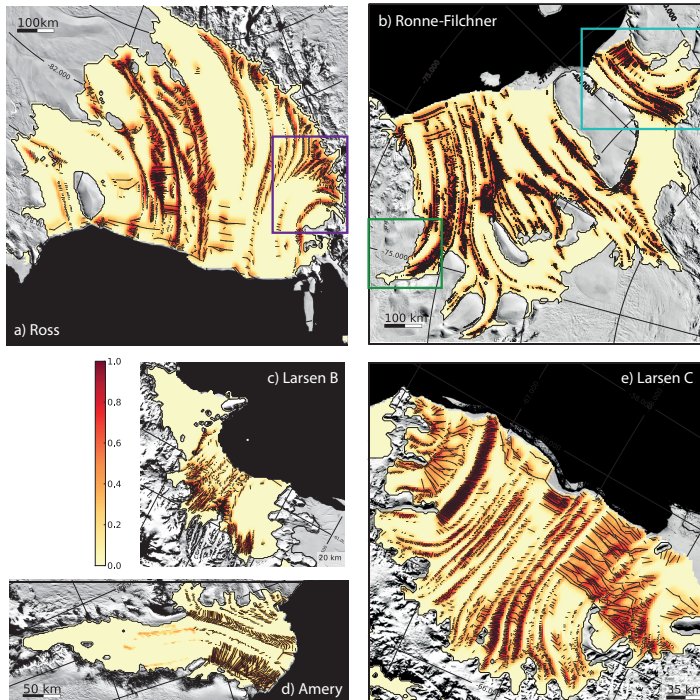


**Fig. 6.** Surface features in the largest Antarctic ice shelves hand-digitized from MODIS data (Scambos et al., 2007, Mosaic of Antarctica). Smoothed observed fracture density  $\phi_{\text{obs}}$  is shaded in orange colors across the ice shelf surrounded by MOA image map. Colored rectangles show area of investigated regional setups.

**Fracture-induced softening in ice dynamics**

T. Albrecht and  
A. Levermann

Title Page

Abstract Introduction

Conclusions References

Tables Figures

⏪ ⏩

⏴ ⏵

Back Close

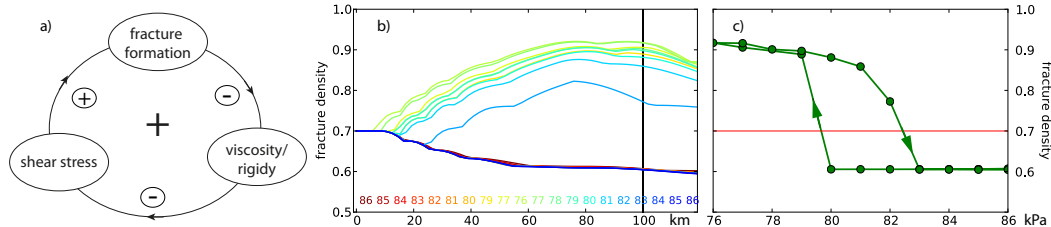
Full Screen / Esc

Printer-friendly Version

Interactive Discussion



## Fracture-induced softening in ice dynamics

T. Albrecht and  
A. Levermann

**Fig. 7.** The self-amplifying feedback **(a)** is studied in a simplified ice-shelf setup for successively varied fracture-initiation threshold  $\sigma_{cr}$ . Corresponding steady-state fracture-density profiles along the flowline are shown in rainbow colors **(b)**. Each profile initiates at the point of prescribed value  $\phi = 0.7$  at the left hand side. Fracture density accumulates or decays with distance from this point depending on the specific threshold. The black vertical line indicates the position 100 km downstream, where values are taken for hysteresis plot **(c)**. Two steady-state fracture densities exist between 79 kPa and 83 kPa depending on the previously evaluated threshold.

Title Page

Abstract

Introduction

Conclusions

References

Tables

Figures

◀

▶

◀

▶

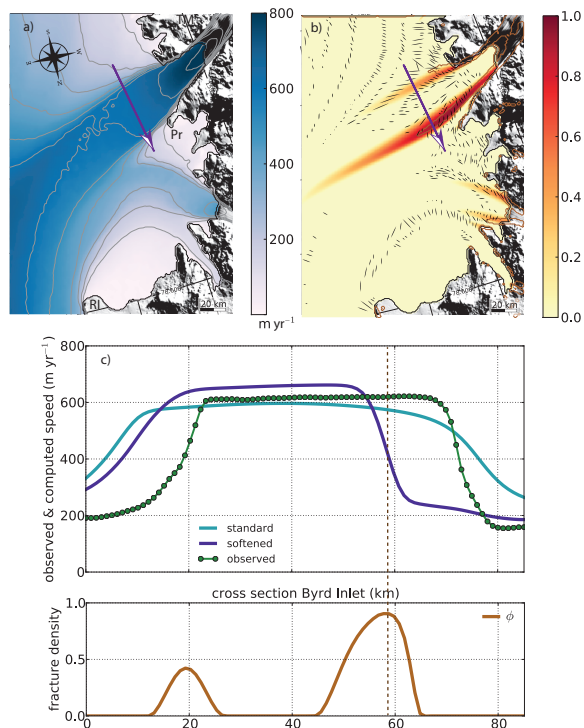
Back

Close

Full Screen / Esc

Printer-friendly Version

Interactive Discussion

Fracture-induced  
softening in ice  
dynamicsT. Albrecht and  
A. Levermann

**Fig. 8.** Observed surface speed of the years 2003 and 2004 **(a)** and modeled steady-state fracture density  $\phi$  **(b)** for the Byrd inlet region in western Ross Ice Shelf (violet box in Fig. 6 a). In the lower panel values of observed (green) and calculated ice speed (blue and violet) as well as corresponding fracture density (brown) are plotted along indicated cross section. Parameters: FESOM-melting factor 0.2,  $E_{SSA} = 0.05$ ,  $\gamma = 0.2$ ,  $\sigma_t = 110$  kPa,  $\gamma_h = 0.05$ ,  $\dot{\epsilon}_h = 20 \times 10^{-10} \text{ s}^{-1}$

Title Page

Abstract

Introduction

Conclusions

References

Tables

Figures

◀

▶

◀

▶

Back

Close

Full Screen / Esc

Printer-friendly Version

Interactive Discussion

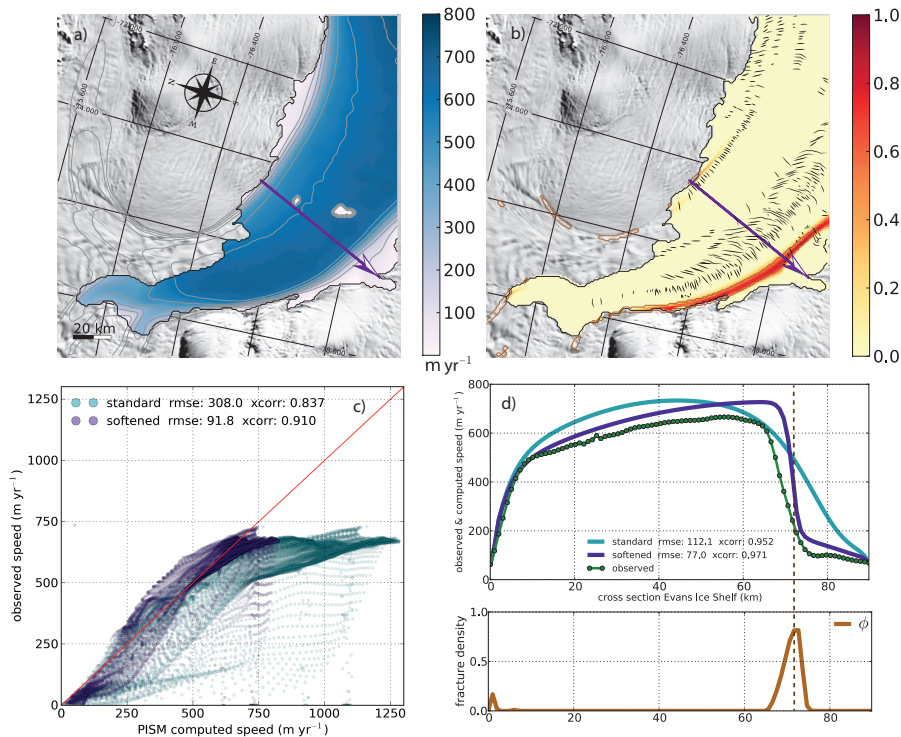


**Fig. 9.** Observed surface speed **(a)** and calculated fracture density **(b)** in the Evans Inlet in western Ronne Ice Shelf (green box in Fig. 6 b). In the lower panels values of observed (green dots) and calculated ice speed are presented, light blue for the constant flow enhancement, violet for fracture-induced softening. Corresponding fracture density (brown) is plotted along the indicated cross section. Parameters: FESOM-melting factor 1.0,  $E_{SSA} = 0.05$ ,  $\gamma = 0.2$ ,  $\sigma_t = 140 \text{ kPa}$ ,  $\gamma_h = 0.1$ ,  $\dot{\epsilon}_h = 12 \times 10^{-10} \text{ s}^{-1}$

Fracture-induced softening in ice dynamics

T. Albrecht and A. Levermann

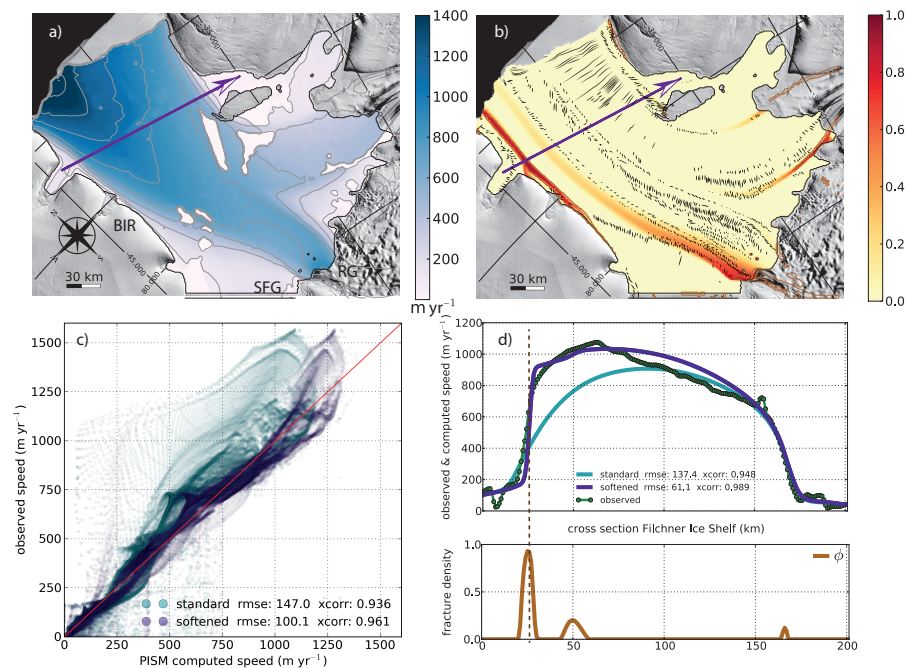


**Fig. 10.** Observed surface speed over MODIS data (a) and calculated fracture density (b) in the Filchner Ice Shelf (light blue box in Fig. 6b). Scatterplot of computed over observed velocities (c) for constant flow enhancement (blue) and in the fracture-softened case (violet). Corresponding cross sections of observed and calculated ice speed as well as fracture density are shown in the lower right panel (d). Parameters: FESOM-melting factor 1.0,  $E_{SSA} = 0.2$ ,  $\gamma = 0.3$ ,  $\sigma_t = 130$  kPa,  $\gamma_h = 0.02$ ,  $\dot{\epsilon}_h = 15 \times 10^{-10} \text{ s}^{-1}$

Title Page

Abstract Introduction

Conclusions References

Tables Figures

◀ ▶

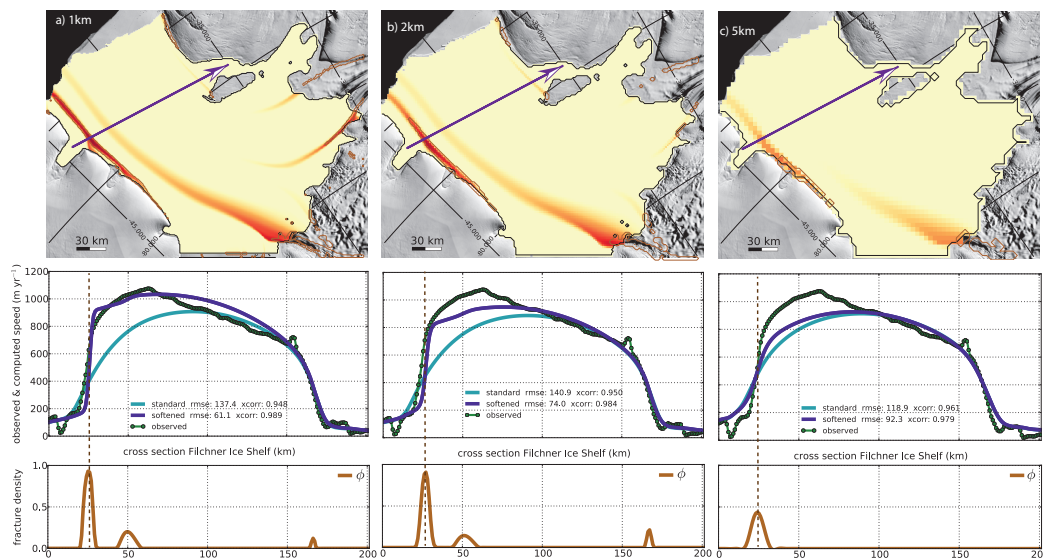
◀ ▶

Back Close

Full Screen / Esc

Printer-friendly Version

Interactive Discussion

Fracture-induced  
softening in ice  
dynamicsT. Albrecht and  
A. Levermann

**Fig. 11.** Calculated fracture density in the Filchner Ice Shelf for varied resolution 1 km, 2 km and 5 km from left to right. In the lower panels values of observed and calculated ice speed as well as the corresponding fracture density are plotted along the indicated cross section. Parameters same as in Fig. 10.

Title Page

Abstract

Introduction

Conclusions

References

Tables

Figures

◀

▶

◀

▶

Back

Close

Full Screen / Esc

Printer-friendly Version

Interactive Discussion

Fracture-induced softening in ice dynamics

T. Albrecht and A. Levermann

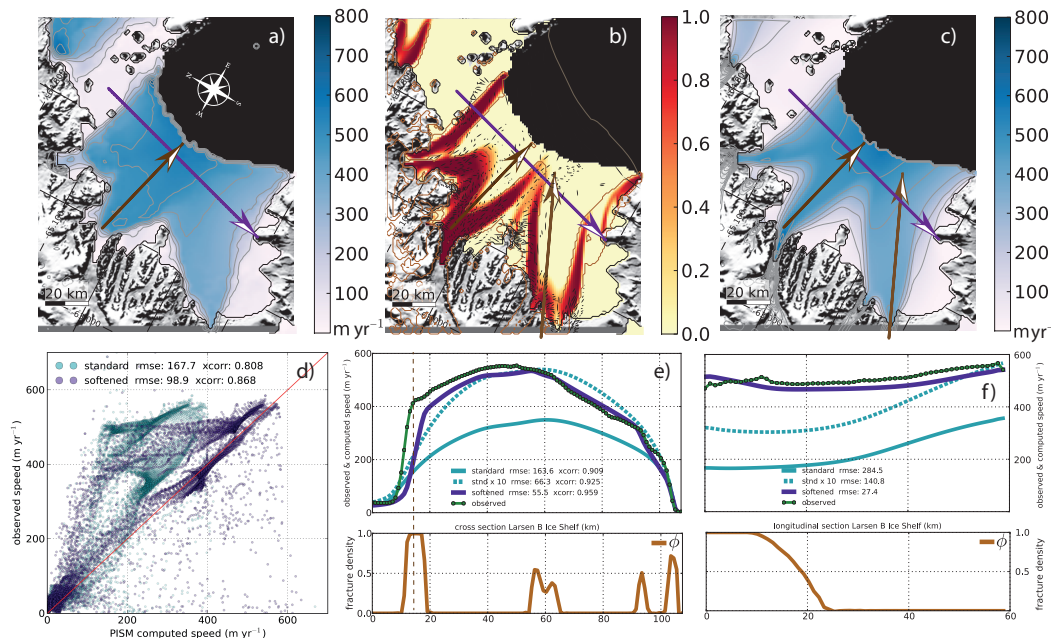


**Fig. 12.** Observed surface speed of the years 1997 to 2000 as well as calculated fracture density and ice speed in the Larsen B Ice Shelf (a–c). Point-by-point correlation of calculated and observed ice velocities in the lower left panel (light blue for constant enhancement factor and violet with fracture-softening). Panels e–f demonstrate the effect of the coupled fracture density on the calculated ice speed (cf. light blue, dashed and violet) compared to observed speeds (green) along indicated transverse section (violet arrow) and longitudinal section (brown arrow). Parameters: FESOM-melting factor 0.2,  $E_{SSA} = 1.0$ ,  $\gamma = 1.0$ ,  $\sigma_t = 60$  kPa,  $\gamma_h = 2.0$ ,  $\dot{\epsilon}_h = 6 \times 10^{-10} \text{ s}^{-1}$

Title Page

Abstract Introduction

Conclusions References

Tables Figures

◀ ▶

◀ ▶

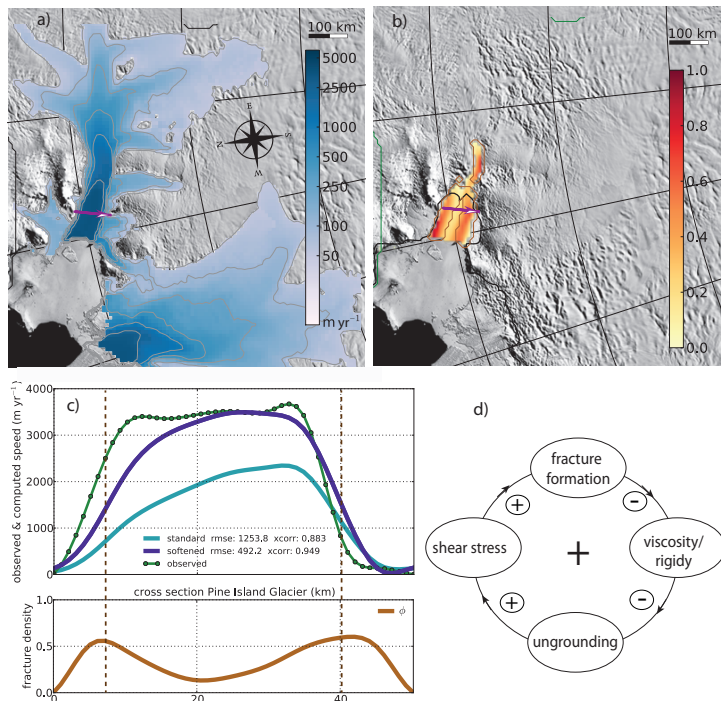
Back Close

Full Screen / Esc

Printer-friendly Version

Interactive Discussion



Fracture-induced  
softening in ice  
dynamicsT. Albrecht and  
A. Levermann

**Fig. 13.** Observed surface speed  $\geq 50 \text{ m yr}^{-1}$  on logarithmic scale **(a)** and calculated fracture density **(b)** in the Pine Island and Thwaites Glacier region. Black contour indicates the modeled grounding line position. Observed and simulated velocity magnitudes are illustrated along the indicated cross section close to the grounding line **(c)**. The associated fracture density is accumulated along the side margins indicated by two smooth maxima. Parameters: PISM melting parameterization,  $E_{\text{SSA}} = 0.8$ ,  $\gamma = 0.3$ ,  $\sigma_i = 96 \text{ kPa}$ ,  $\gamma_h = 0.01$ ,  $\dot{\epsilon}_h = 100 \times 10^{-10} \text{ s}^{-1}$ . A sketch of a potentially positive feed-back loop indicates “ungrounding” and hence grounding-line retreat as additional amplifying effect **(d)**.

Title Page

Abstract

Introduction

Conclusions

References

Tables

Figures

◀

▶

◀

▶

Back

Close

Full Screen / Esc

Printer-friendly Version

Interactive Discussion